16th World Congress in Computational Mechanics (WCCM)
21-26 July 2024, Vancouver, Canada
A. Korobenko, M. Laforest, S. Prudhomme, R. Vaziri (Eds)

POWER DISSIPATION MODELLING IN WHEEL-RAIL CONTACT

ANDRZEJ M. MYŚLIŃSKI[1], ANDRZEJ J. CHUDZIKIEWICZ[2]

[1] Systems Research Institute
ul. Newelska 6, 01-447 Warsaw, Poland
myslinsk@ibspan.waw.pl

[2] University of Radom
ul. Malczewskiego 29, 26-600 Radom, Poland
andrzej.chudzikiewicz@gmail.com

Key words: Rolling contact, Elasto-plastic material, Energy dissipation, Wear.

Abstract. This paper is concerned with the modeling of power dissipation due to friction and its relation with wear estimation in wheel–rail contact. In contact models, wear is usually described in terms of the wear depth function. This function modifies the gap between the contacting bodies as well as the shape of the surfaces of the wheel and rail in contact. In this paper, besides the wear depth function, the dissipated energy, rather than the contact stress, is taken into account to evaluate the wear impact on rail or wheel surfaces. The dissipated energy allows us to more precisely evaluate the wear debris amount as well as the depth of wear and its distribution along the contact interface. A two-dimensional rolling contact problem with frictional heat flow is considered. The elasto-plastic deformation of the rail is assumed. This contact problem is governed by a coupled system of mechanical and thermal equations in terms of generalized stresses, displacement and temperature. The finite element method is used to discretize this problem. The generalized Newton method is applied to numerically solve this mechanical subproblem. The dissipated power is evaluated based on the resultant force and slip at a reference point. Numerical results including the distribution of slip velocity, power factor and wear rate are provided and discussed.

1 INTRODUCTION

The contact occurring between the wheel moving over the rail is characterized by high stress in contact patch, creep distribution as well as the friction phenomenon. It can lead to the gradually wear of surfaces and deterioration of wheel and rail operational conditions [1]. Rolling contact fatigue phenomenon is frequently observed in the rolling contact. This phenomenon caused by high alternating stress field in the contact area leads to material removal driven by crack propagation. This phenomenon also accounts for wheel squeal noise [2]. This unpleasant noise occurring mainly due to lateral creepage is troublesome in densely populated areas.

Wear phenomenon is described as a gradual removal or deformation of material from the surface of solid body subjected to physical or chemical factors [1, 3]. This phenomenon may be

generated by corrosion, repeated cyclical rubbing between two surfaces, or different chemical factors. Although many different wear laws are formulated in literature or used in industry, they can be divided into two groups [1]. The first approach to formulate the wear law is based on the equations relating normal loads and the amount of the worn material. The other approach consists in evaluating the volume of the worn material as proportional to energy or power dissipated due to friction forces at the contact interface. Both approaches can be also considered either as global or local wear laws. Global form of the wear law leads to estimation of the volume of the worn material based on calculation of global forces and creepage along the contact interface [1].

The wear evolution process of wheels and rails is slowly strongly nonlinear phenomenon. From experimental or numerical tests [1, 5, 6] it follows that this process depends on many variables including operating conditions, initial profiles, contact and friction conditions, stresses and their distribution, temperature, materials or surface properties and parameters. Since these factors are changing during the wheel movement, so the friction coefficient as well as friction energy are changing. Analysis of different parameters influencing the evolution of wear process as well as the results of experiments allow the researchers to formulate many different wear prediction models available in literature [1, 3, 5, 7]. Rolling contact problems with friction and/or heat flow are intensively studied in literature [14, 15, 16].

In this paper we shall use and implement power dissipation model combined with Archard model to compute wear rather than classic Archard model [1] only. Recall from [8, 9], since the wear distribution updates the contact geometry, it causes that numerical modelling of contact problems is not easy and generates interest in developing new methods. The friction is governed by Coulomb model [1]. Moreover heat flow due to friction is also taken into account [11]. We focus on power dissipation modelling rather than stresses as in [16]. This work develops new approach to estimate numerically power dissipation and wear modelling in wheel - rail contact problems and provides new insights into the research of these problems. Elasto-plastic deformation of rail material is assumed. Wear estimation is based on combined power dissipation and Archard models rather than Archard model only. The simulation of the discretized contact problem is based on generalized Newton method [17] rather than Fastsim or Contact software methods [19]. The update finite element mesh algorithm related to the worn material volume rather than general type algorithm is used. Based on numerical results a few conclusions are formulated. Contact patches obtained for elasto-plastic case are characterized by longer zones and lower stress intensity than in the elastic case. For relative small increase of temperature the contact patches are slightly longer than for plasto-elastic model. The power dissipated as well as the wear rate are strongly dependent on the friction coefficient, i.e. they increase when the friction coefficient increases.

2 WHEEL-RAIL CONTACT PROBLEM

Let us consider two-dimensional rolling contact problem (see Fig. 1). The rail strip occupies two-dimensional domain $\Omega \subset R^2$ and is located on a rigid foundation. The strip is subject to elasto-plastic deformation by the wheel rolling along the upper surface of the strip and pressed

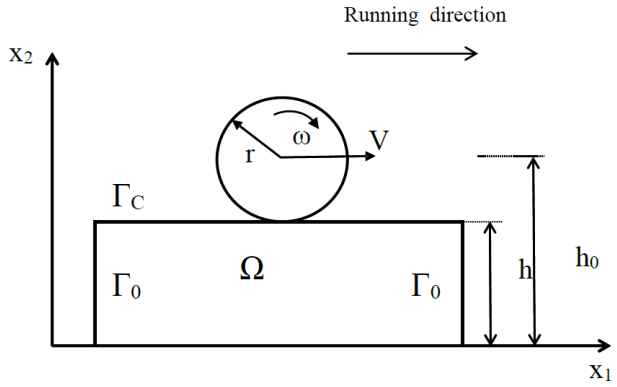

Figure 1: Rolling contact problem.

into it. Geometrical parameters $h > 0$ and $r_0 > 0$ denote, respectively, the height of the strip and the radius of the wheel. Since the wheel is pressed into the strip it means that the distance h_0 of wheel axis from rail upper surface satisfies geometrical condition $h_0 < h + r_0$. The strip is assumed to be suitably long, i.e., it has much bigger length comparing to the wheel radius r_0. The strip is clamped along both vertical edges. By Γ we denote the boundary of domain Ω. It consists from two sub-boundaries Γ_0 and Γ_C such that their intersection is an empty set. The contact between the wheel and the strip appears along the boundary Γ_C and is described by imposed contact non-penetration and friction conditions. Denote the strip displacement and its absolute temperature by u and θ, respectively. Both functions are dependent on spatial variable $x = (x_1, x_2) \in \Omega$ and time variable $t \in [0, T]$, $T > 0$ is a given constant, i.e. we shall write $u = u(x, t) = (u_1, u_2)$ and $\theta = \theta(x, t)$. The strip deformation under moving loading is characterized in terms of Cauchy stress tensor and linearized strain tensor [20] denoted, respectively by, $\sigma = \{\sigma_{ij}\}, i, j = 1, 2$, $\sigma_{ij} = \sigma_{ji}$ and $\varepsilon^e(u) = \{\varepsilon^e_{ij}(u)\}$. The Cauchy stress tensor and the elastic strain tensor are related by the Hooke's law. Strip mass density we shall denote by ρ. Moreover, λ as well as γ are Lamé coefficients of the strip material [19, 20]. The thermal expansion and the heat capacity coefficients are denoted by α and c_p, respectively. Moreover by div $\sigma(u)$ we denote the divergence operator div $\sigma(u)$ of stress. The elasto-plastic deformation of the strip is governed by the additive small strain plasticity model [20]. Von Mises yield function is used to define the set of admissible stresses. The stress σ is assumed to satisfy the consistency condition [20]. For a given temperature θ, the displacement u, the stress σ satisfies in domain Ω and in time interval $(0, T)$ the governing equation:

$$\rho c_p \frac{\partial^2 u}{\partial t^2} = \text{div}\sigma - \alpha(3\lambda + 2\gamma)\nabla\theta, \tag{1}$$

The following boundary conditions are imposed on the displacement u:

$$u = 0 \ \text{ on } \ \Gamma_C \quad \text{and} \quad \sigma \cdot n = F \ \text{ on } \ \Gamma_C. \tag{2}$$

Normal traction vector $F = (F_1, F_2)$ is a priori not known. This vector follows from conditions of non-penetration and friction imposed on contact sub-boundary Γ_C [8, 14].

$$u_2 + \tilde{h}_r + w \leq 0, \quad F_2 \leq 0, \quad (u_2 + \tilde{h}_r + w)F_2 = 0. \tag{3}$$

$$|F_1| \leq \mu |F_2|, \quad F_1 du_1 \leq 0, \quad (|F_1| - \mu |F_2|)du_1 = 0, \tag{4}$$

In (3), $\tilde{h}_r$ and w denote, respectively, the gap between the wheel and rail as well as wear depth function. From contact geometry it follows that the gap function is equal to $\tilde{h}_r = h - h_0 + \sqrt{r_0^2 - (u_1 + x_1)^2}$. The wear depth function w is determined on the contact interface on obeys Archard's law (12). μ is a friction coefficient. Due to the work of friction forces the heat energy is generated during the wheel movement. In turn it generates the changes of the rail temperature θ. We assume that the heat transfer is due to conductivity only. Since the wheel moves along the rail this heat flow is also not stationary. So, the strip temperature evolution is determined by non stationary heat conductive equation. Let us denote by $\bar{\kappa}$ a thermal conductivity coefficient. Therefore, temperature θ in (1) in time interval $(0, T)$ and in the strip domain Ω is governed by heat conduction equation:

$$\rho c_p \frac{\partial \theta}{\partial t} = \bar{\kappa} \triangle \theta. \tag{5}$$

In time interval $(0, T)$ the temperature function θ satisfies also the boundary condition along the boundary Γ:

$$\bar{\kappa} \frac{\partial \theta}{\partial n} = Q \ \text{ on } \ \Gamma_C \quad \text{and} \quad \bar{\kappa} \frac{\partial \theta}{\partial n} = 0 \ \text{ on } \ \Gamma_0. \tag{6}$$

Heat flux function Q is generated due to frictional force. This function is determined by the friction coefficient, friction force, sliding velocity. It also depends on the thermal material resistance coefficient. We shall assume function Q is stationary.

2.1 Wear evaluation models

We shall consider abrasive wear only. In this type of wear the worn material in the form of wear debris is assumed to be shifted away from the gap between the bodies. The worn and removed material updates the location and geometry of the contacting surfaces. It implies that the position and shape of the contacting surfaces is also updated. The modification of contact interface leads finally to update of tangential and normal forces along the contact patch. In turn, it causes the modification of wear process and gap between the bodies. Due to this complex relation between contact geometry and forces modelling of the contact problems with wear is recognized as challenging task [8].

2.1.1 Dissipated energy wear model

In literature there are proposed many wear laws based on evaluation of the dissipated energy due to work of the friction force. These formulations include, among others, Zobory, Krause-Poll, BRR and USFD wear laws [1, 5]. In this approach the removed material volume Vol is

estimated. The amount of the removed material directly depends on the frictional work and is calculated using the formula:

$$Vol = \begin{cases} \alpha_f E_f & P_f/A \leq \pi_{lim} \\ k_{sm}\alpha_f E_f & otherwise \end{cases} \tag{7}$$

where $k_{sm} > 0$, $A > 0$ and $\pi_{lim} > 0$ denote a proportionality constant, contact patch area and a threshold value, respectively. In (7) the estimated experimentally wear constants $\alpha_f > 0$ and $\alpha_s = k_{sm}\alpha_f >$ are associated, respectively, with mild and severe wear regimes. The frictional work E_f may be estimated from the frictional power P_f and time integration step $\triangle t$ as follows:

$$E_f = P_f \triangle t \quad \text{and} \quad P_f = T\gamma \cdot V = (\mid F_x\zeta \mid + \mid F_y\eta \mid + \mid M_z\omega \mid) \cdot V \tag{8}$$

The power P_f is calculated as the product of velocity V as well as force $F = [F_x, F_y]$ and creepage $\zeta = [\zeta_x, \zeta_y]$ consisting from longitudinal and lateral components. Moreover in 3D case the product of spin moment M_z and spin creepage ω is added. The energy wear coefficient α_f is determined experimentally [1] and belongs to rail material parameters. Its range of applicability is large [1]. In order to evaluate the total dissipated energy E_f let us consider first one cycle of the movement of the frictional force F_1 from point x_{1min} to point x_{1max} of the contact interface during time interval $(t - \triangle t, t)$. Using formula (4), the energy E_{f^i} dissipated in one slip cycle i is equal to the product of friction force and sliding distance according to the formula:

$$E_{f^i} = \int_{t-\triangle t}^{t} \mid F_1 \mid dx_1 = \int_{t-\triangle t}^{t} \mu \mid F_2 \mid dx_1 = \mu \mid F_2 \mid (x_1(t) - x_1(t - \triangle t)), \tag{9}$$

Since in formula (9) the history of sliding displacement is used, it makes it very useful in energy modelling for bodies in contact subject to plastic deformation. Summing energies dissipated in each cycle we obtain the formula describing the total dissipated energy E_f as equal to

$$E_f = \alpha_f \sum_i E_{f^i} \tag{10}$$

We shall refer to the system (9)-(10) as the description of the global dissipated energy method [8].

2.1.2 Wear depth evaluation

Nowadays, Archard's wear law [7] seems to be most frequently used wear law. According to it the volume of the worn material is dependent on the wear coefficient, normal force and sliding velocity divided by the hardness of the softer contact material. The wear coefficient is calculated experimentally. In literature can be found different estimations of wear coefficients. In USFD wear model the wear rate is the function of $T\gamma$ index. The wear rate is linear and constant for small and medium values of this index, respectively, and is rapidly increasing for

high values of this index. From the local wear analysis [8] it follows that the local wear depth function $w = w(x)$ can be estimated from the total dissipated energy:

$$w = \alpha_w E_f. \tag{11}$$

The local energy wear coefficient $\alpha_w > 0$, appearing in (11) as proportionality coefficient, is determined experimentally and belongs to rail material parameters [1]. This coefficient is usually set as equal to $\alpha_w = \alpha_f$, especially for a unit contact patch [1]. From (9) and (11) we may estimate also the wear rate function dw as equal to

$$dw = \alpha_w \mu \mid F_2 \mid du_1. \tag{12}$$

The wear rate law (12) relating the increment of the wear depth with longitudinal velocity du_1, normal pressure F_2 represents the classical Archard wear law [7]. This function appears also in the condition (3) and can be called the inner variable. Since it updates the gap between the bodies in contact, so it also updates the solution of contact problem (1)-(4). The system (1)-(6) and (10)-(12) consisting from equations as well as equality and inequality type boundary conditions governs the thermo-elasto-plastic wheel-rail contact problem in terms of displacement, generalized stresses and temperature. In order to estimate the dissipated power and wear we shall solve it numerically. Finite element and finite difference methods have been used to obtain finite dimensional formulation of this system.

3 NUMERICAL ALGORITHM

In the literature, there are many proposed numerical models and methods to implement wear laws as well as to calculate wheel–rail energy dissipation and wear (see the references in review papers [1, 5]). All these approaches are facing and trying to solve the same challenges consisting in the mutual dependence between the simulated dynamical model and rail or wheel profiles altered due to wear. Nowadays, most frequently, a two-step approach is used. First, for a given profile, a vehicle dynamic problem is solved and then updated due to the wear geometry of profiles being calculated. Next, for a given updated profile from the previous step, a dynamic problem is solved.

In the rolling contact problem (1)–(6) and (10)–(12), the calculated contact traction and wear depth depend on the thermal distortion of the wheel and the rail strip. On the other hand, the heat flow as well as the temperature achieved by the strip directly depend on contact pressure and on the rail profile. So, it is a system of coupled equations governing the thermo-elasto-plastic contact problem. Numerically, either we can solve mechanical and thermal equations simultaneously, i.e., in the same time instant, or we can decouple this system of equations and solve them sequentially in time. Since the second strategy is easier to implement, it has been used.

The wear evaluation algorithm in time instant t and the consecutive time instant $t + dt$, where dt denotes the time increment, is displayed on Figure 2. Assume the temperature θ^t at time t is given. For time t, the mechanical subsystem (1)–(4) is solved and normal contact traction

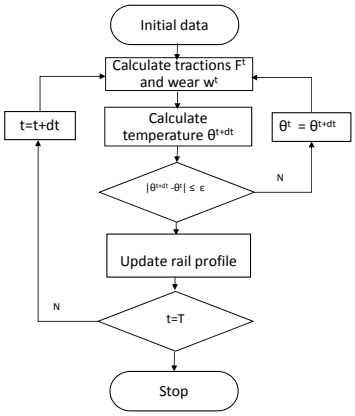

Figure 2: Wear evaluation algorithm.

F_2^t and wear w^t are evaluated. Based on it, the computations in the next time instant $t + dt$ are executed. In this step, the thermal system (5) and (6) is solved, and the temperature θ^{t+dt} at time $t + dt$ is calculated. The heat flux Q^{t+dt} at time step $t + dt$ in (6) is calculated as a time instant from formula $Q^{t+dt} = \mu V F_2^t$ using traction force calculated in the previous time step. The solution of the thermo-mechanical system is stopped if the difference in temperatures calculated in consecutive time instants satisfies:

$$\mid \theta^{t+dt} - \theta^t \mid \leq \epsilon, \tag{13}$$

for a given suitable small $\epsilon > 0$. The stopping condition (13) means that the temperature has reached a stable state and is almost constant. In the case that this condition is not satisfied, for a new calculated temperature θ^{t+dt} at time step $t + dt$, the mechanical subsystem (1)–(4) is solved. When the thermo-mechanical system (1)–(6) is solved, the worn volume material Vol^t is evaluated based on (9)–(12) and an update of the rail profile is calculated.

4 NUMERICAL RESULTS

The distribution of the dissipated power and temperature as well as the evolution of the wear depth and the worn material in the wheel–rail system (1)–(12) were estimated numerically. The MATLAB programming environment was used to realize computations. Domain Ω occupied by the strip was taken as rectangular in R^2:

$$\Omega = \{x = (x_1, x_2) \in R^2 : x_1 \in (-a, a), x_2 \in (0, b)\}. \tag{14}$$

with $a = 20$ and $b = 10$. The finite element method was used to replace domain Ω with finite elements. It was divided into 1240 quadrilateral elements. Each element had eight nodes. The mesh was adapted to ensure good accuracy. In the contact area, the finest mesh was used. Far

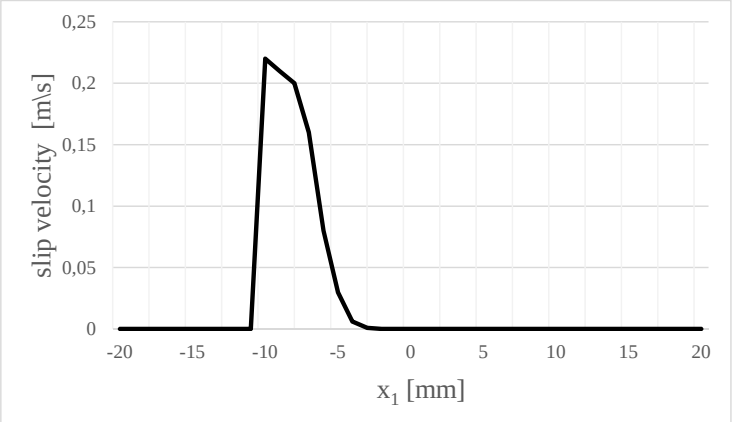

Figure 3: Slip velocity distribution over the strip.

from this area, the mesh was coarser. In the computations, the velocity V, radius of the wheel r_0 and the friction coefficient μ were, respectively, set to V = 25 m/s, r_0 = 0.46 m and μ = 0.5. The thermal resistance coefficient r = 1000 KNs/J was used. A force equal to 96 kN was applied to what is equivalent to the penetration of the wheel equal to $\delta = 0.1 \cdot 10^{-3}$ m. The temperature of the outside air was set to θ_g = 20 °C.

4.1 Distribution of Dissipation Power

Figures 3 and 4 display, respectively, the slip velocity and power factor distributions in the x_1 direction along the contact interface. Figure 3 shows the slip velocity distribution. This graph indicates that this velocity is nonsmooth. It is rapidly increasing to reach the maximum value and next rapidly decreasing to zero. Reports in [19] indicate that the calculation of this velocity is strongly dependent on the mesh size. The power factor p_w along the x_1 axis is defined as follows:

$$p_w(x_1, x_2) = p(x_1, x_2) \cdot v(x_1, x_2), \tag{15}$$

where p and v denote, respectively, contact pressure and slip velocity. The power factor (15) measures the power dissipated but is slightly different than the product of tangential stress and slip velocity. The contact pressure is calculated based on (1)–(8). The friction power appears when the wheel enters the contact zone, increases to reach the maximum and next decreases to zero when the wheel goes outside the contact zone. As reported in [19], the transversal stress is higher for the elastic than for the elasto-plastic model. For these two materials, the peaks of this stress are also differently located. The contact zone is longer for elasto-plastic than for elastic materials. The distributions of slip velocity as well as power factor displayed in Figures 3 and 4 are in accordance with physical reasoning and are comparable to distributions obtained in [19] using other methods.

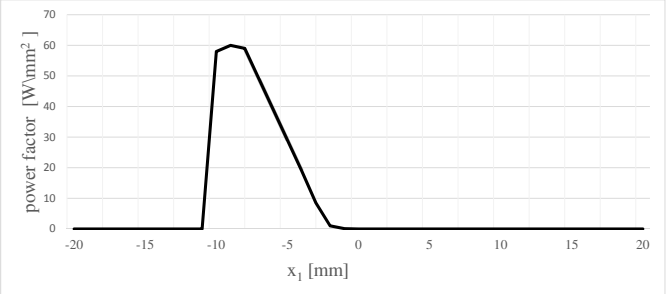

Figure 4: Power factor distribution on the contact patch.

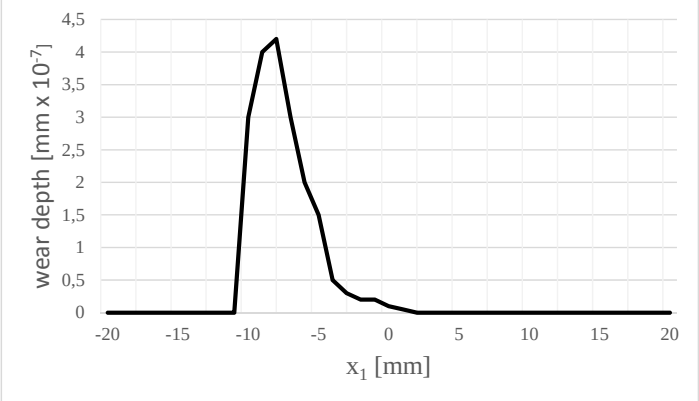

Figure 5: Wear depth distribution.

4.2 Wear Depth Distribution

The wear depth distribution over the contact patch, displayed in Figure 5, was calculated using (7)–(12). When the contact starts, the wear depth grows smoothly and quickly, and a large amount of worn material is removed. When the wheel is approaching the end of the contact zone, the wear depth function rapidly decreases.

Remark: due to the regular wear map, this graph is also regular. Discontinuous wear maps may also generate discontinuous wear depth distributions. Figure 6 displays the dependence of the power dissipation on the friction coefficient. The amount of dissipated power is strongly correlated with the change in the friction coefficient. For higher values of the friction coefficient, the dissipated energy amount is also higher. It implies that the creep force and creepage are also increasing when the friction coefficient is increasing. Since the wear rate is strongly dependent on the power dissipation by means of the friction work, the dependence of wear on the friction coefficient is similar to that found in the power dissipation results in Figure 6. The data in Figure 7 confirm this expectation.

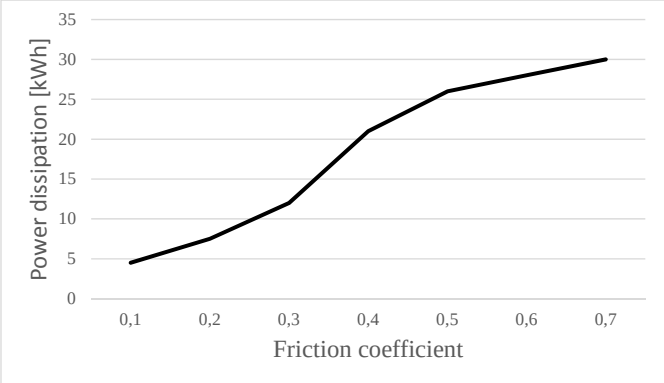

Figure 6: The dependence of power dissipation on friction coefficient.

The method to solve the mechanical subsystem (1)–(4) is quickly convergent. It required 30 iterations to find the solution of this system. At the beginning of iterations, the active sets were calculated not precisely, and they changed during iterations. Closer to the final solution, these sets were stable, which ensures convergence.

5 CONCLUSIONS

Besides Archard's wear model, in the paper, the power dissipation approach has been used to estimate the wear phenomenon and its impact on wheel–rail elasto-plastic contact with frictional heat flow. This approach combined with the application of semi-smooth Newton and Cholesky methods to numerically solve contact problems allows us to follow the modification of the dissipated power, the wear depth distributions as well as the location of the contact surfaces. From numerical results, it follows that, in the elasto-plastic case, the calculated contact patches are longer than in the elastic case. Moreover, the contact stress is also lower than in the elastic case. The power dissipated as well as the wear rate are strongly dependent on the friction coefficient. Moreover, the obtained results confirm the robustness and efficiency of the proposed method,

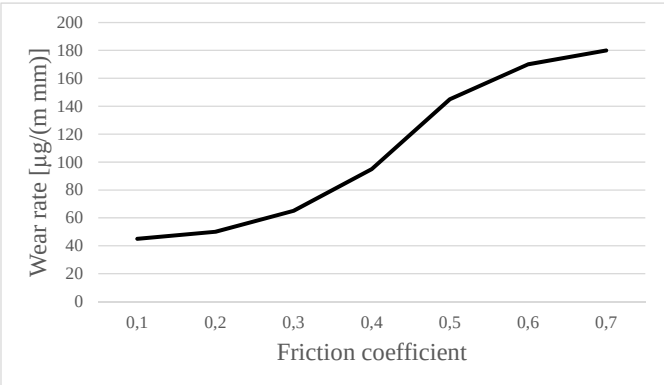

Figure 7: The wear rate as a function of friction coefficient.

including the update of the contact interface location and geometry, in estimation of the wear distribution along the contact patch. On the other hand, this research indicates problems which are not fully clear and will be the subject of future research. The dependence of the wear process on hardening as well as temperature and material parameters requires additional research. The computations for 3D wheel–rail contact are planned to be executed. Future research will also include the treatment and investigation of the wear evolution process in terms of the shape optimization problem. The location and shape of the contact area may be considered as a design variable [21]. The volume of the worn material or the dissipated power may be chosen as an optimization criterion. The calculated wheel or rail parameters will ensure the minimal volume of the removed material.

REFERENCES

[1] Bosso, N., Magelli, M., Zampieri, N. Simulation of wheel and rail profile wear: a review of numerical models. *Rail. Eng. Science* (2022), **30(4)**:403–436.

[2] Omasta, M., Navrátil, V., Gabriel, T., Galas, R., Klapka, M. Design and development of a twin disc test rig for the study of squeal noise from the wheel-rail interface. *Applied Engineering Letters* (2022), **7**(1):10-16.

[3] Liu, H., Yang, B., Wang, C., Han, Y., Liu, D. The mechanisms and applications of friction energy dissipation. *Friction* (2022), **11**(6):839-864.

[4] Al-Maliki, H., Meierhofer, A., Trummer, G., Lewis, R., Six, K. A new approach for modelling mild and severe wear in wheel-rail contacts. *Wear* (2021), **476**:203761.

[5] Meng, H.C., Ludema, K.C. Wear models and predictive equations: their form and content. *Wear* (1995), **181–183**:443–457.

[6] Yang, Z., Zhang, P., Moraal, J., Li, Z. An experimental study on the effects of friction modifiers on wheel–rail dynamic interactions with various angles of attack. *Rail. Eng. Science* (2022), **30**(3):360-382.

[7] Harmon, M., Lewis, R. Review of top of rail friction modifier tribology. *Tribology: Materials, Surfaces and Interfaces* (2016), **10**(3):150–162.

[8] Doca, T., Andrade Pires, F.M. Finite Element Modelling of Wear using the Dissipated Energy Method coupled with a Dual Mortar Contact Formulation. *Computers and Structures* (2017), **191**:62–79.

[9] Fouvry, S., Paulin, C. An effective friction energy density approach to predict solid lubricant friction endurance: Application to fretting wear. *Wear* (2014), **319**:211–226.

[10] Abdo, J. Materials Sliding Wear Model Based on Energy Dissipation. *Journal of Mechanics of Advanced Materials and Structures* (2015), **22**(4):298–304.

[11] Alarcon, G.I., Burgelman, N., Meza, J. M., Toro, A., Li, Z. Power dissipation modeling in wheel/rail contact: Effect of friction coefficient and profile quality. *Wear* (2016), **366-367**:217-224.

[12] Ramalho, A., Miranda, J.C. The relationship between wear and dissipated energy in sliding systems. *Wear* (2006) ,**260**(4/5):361-367.

[13] Faccoli, M., Petrogalli, C., Lancini, M., Ghidini, A., and Mazzu, A. Rolling Contact Fatigue and Wear Behavior of High-Performance Railway Wheel Steels Under Various Rolling-Sliding Contact Conditions. *Journal of Materials Engineering and Performance* (2017), **26**(7):3271-3284.

[14] Myśliński, A., Chudzikiewicz, A. Power dissipation modeling in wheel-rail contact. *Applied Sciences* (2024), **14**(1):165.

[15] Naeimi, M., Li, S., Li, Z., Wu, J., Petrov, R., Sietsma, J., Dollevoet, R. Thermomechanical analysis of the wheel-rail contact using a coupled modelling procedure. *Tribology International* (2018), **117**:250–260.

[16] Myśliński, A., Chudzikiewicz, A. Wear modelling in wheel-rail contact problems based on energy dissipation. *Tribology - Materials, Surfaces and Interfaces* (2021), **15**:138–149.

[17] Liu, B., Bruni, S. Application of the extended FASTSIM for non-Hertzian contacts towards the prediction of wear and rolling contact fatigue of wheel/rail systems. *Proceedings of the Institution of Mechanical Engineers, Part F: Journal of Rail and Rapid Transit.* (2024), **238**(4):427-436. doi:10.1177/09544097231178857.

[18] Meacci, M., Shi, Z., Butini, E., Marini, L., Meli, E., Rindi A. A railway local degraded adhesion model including variable friction, energy dissipation and adhesion recovery. *Vehicle System Dynamics* (2021), **59**(11):1697–1718, doi: 10.1080/00423114.2020.1775266.

[19] Hager, C., Wohlmuth, B. I. Nonlinear complementarity functions for plasticity problems with frictional contact. *Comput. Methods Appl. Mech. Engrg.* (2009), **198**:3411–3427.

[20] Han, W., Reddy, B.D. *Plasticity. Mathematical Theory and Numerical Analysis*, 2nd edition, New York, Springer, USA, (2013).

[21] Myśliński, A., Wróblewski, M. Structural optimization of contact problems using Cahn-Hilliard model. *Computers and Structures* (2017), **180**:52–59.